THEORETICAL CLUES TO THE ULTRAVIOLET DIVERSITY OF TYPE Ia SUPERNOVAE

Peter J. Brown[1], E. Baron[2], Peter Milne[3], Peter W. A. Roming[4,5], and Lifan Wang[1]

[1] George P. and Cynthia Woods Mitchell Institute for Fundamental Physics & Astronomy, Texas A. & M. University, Department of Physics and Astronomy, 4242 TAMU, College Station, TX 77843, USA; pbrown@physics.tamu.edu
[2] Homer L. Dodge Department of Physics and Astronomy, University of Oklahoma, 440 W. Brooks, Rm 100, Norman, OK 73019-2061, USA
[3] Steward Observatory, University of Arizona, Tucson, AZ 85719, USA
[4] Southwest Research Institute, 6220 Culebra Road, San Antonio, TX 78238, USA
[5] University of Texas at San Antonio, 1 UTSA Circle, San Antonio, TX 78249, USA

ABSTRACT

The effect of metallicity on the observed light of Type Ia supernovae (SNe Ia) could lead to systematic errors as the absolute magnitudes of local and distant SNe Ia are compared to measure luminosity distances and determine cosmological parameters. The UV light may be especially sensitive to metallicity, though different modeling methods disagree as to the magnitude, wavelength dependence, and even the sign of the effect. The outer density structure, ^{56}Ni, and to a lesser degree asphericity, also impact the UV. We compute synthetic photometry of various metallicity-dependent models and compare to UV/optical photometry from the *Swift* Ultra-Violet/Optical Telescope. We find that the scatter in the mid-UV to near-UV colors is larger than predicted by changes in metallicity alone and is not consistent with reddening. We demonstrate that a recently employed method to determine relative abundances using UV spectra can be done using UVOT photometry, but we warn that accurate results require an accurate model of the cause of the variations. The abundance of UV photometry now available should provide constraints on models that typically rely on UV spectroscopy for constraining metallicity, density, and other parameters. Nevertheless, UV spectroscopy for a variety of supernova explosions is still needed to guide the creation of accurate models. A better understanding of the influences affecting the UV is important for using SNe Ia as cosmological probes, as the UV light may test whether SNe Ia are significantly affected by evolutionary effects.

Key words: distance scale – methods: numerical – supernovae: general – supernovae: individual (SN2011by, SN2011fe) – ultraviolet: general

1. THE INFLUENCE OF METALLICITY ON TYPE IA SUPERNOVAE

Supernovae are important cosmological tools for measuring the expansion history of the universe (Riess et al. 1998; Schmidt et al. 1998; Perlmutter et al. 1999; Suzuki et al. 2012; Ganeshalingam et al. 2013). Their usefulness as standardizable candles (see Branch 1998; Leibundgut 2001) requires the relationships between the luminosity and the observed color and light curve shape to be the same for supernovae (SNe) at all redshifts. One major concern is that evolution in the properties of the progenitors with redshift will systematically change their luminosity and lead to incorrect distance measurements. One property expected to change with redshift is the average metal content (mass fraction of elements heavier than helium) of the universe and its constituents as stars form from the elements created in the lives and deaths of previous generations of stars. We will refer to the metal content generically as "metallicity" but will clarify as appropriate the specific elemental ratios or abundances.

Metallicity could affect the progenitor system and explosion (including the SN observables) at all times leading up to, during, and after the explosion. The premordial metallicity at the time of the SN progenitor formation could affect the evolution of the SN progenitor into a white dwarf and its final C/O ratio and central density (Umeda et al. 1999). It could affect the mass lost by the accreting white dwarf through winds (Kobayashi et al. 1998). The metallicity of the donated material could change the metallicity of the outer layers of the white dwarf. The metallicity of the WD could affect its final density structure. The electron fraction (influenced by the amount of ^{22}Ne present in the progenitor) affects the relative abundances of ^{56}Ni (which powers the luminosity), ^{58}Ni, and ^{54}Fe (Mazzali & Podsiadlowski 2006; Höflich et al. 2013). The final metallicity (and its spatial variation) within the ejecta could be affected not just by the primordial metallicity but by the amount of nucleosynthetic products of the explosion and the degree to which they are mixed.

By its observational nature, astrophysicists cannot change the initial conditions of actual stars and observe how their explosions and observable characteristics respond. Instead, theoretical models are made from the best available knowledge of conditions and physical properties. The ways that metallicity can be incorporated into theoretical models vary greatly. Höflich et al. (1998) modified the pre-explosion metal content and examined the effect on light curves. Lentz et al. (2000) attempted to replicate this in a radiation transport simulation by scaling the amount of elements heavier than oxygen in the unburned layers and the amount of ^{54}Fe in the incomplete burning zone. Timmes et al. (2003) studied the relationship between Z and the ^{56}Ni mass (and thus the luminosity). Sauer et al. (2008) tested the effect of varying the amount of stable Fe, ^{56}Ni, and Ti and Cr together. Bravo et al. (2010) changed the metallicity Z in the pre-main-sequence model, evolved it and exploded it to study the mass of ^{56}Ni ejected, the corresponding bolometric luminosity, and the effect on the luminosity-width relation. Most of these studies show that the effect of changing heavy metal abundances is the strongest at UV wavelengths (Lentz et al. 2000; Sauer et al. 2008; Walker et al. 2012).

Observationally, many studies have looked for "metallicity" or similar effects in the properties of SNe by comparing with properties of the host galaxy. Most focus on two properties of SNe—their peak luminosity (which is correlated with the light curve shape) and the difference between the peak luminosity and that expected based on the light curve shape. The latter is often given in terms of Hubble residuals (HR), defined as the difference between the redshift distance modulus (calculated using the redshift of the host galaxy and the best fit cosmology) and the luminosity distance modulus (calculated from the SN flux and light curve shape). Gallagher et al. (2005) found no correlation between emission line metallicity of star forming host galaxies and the SN luminosity and a low significance correlation with HR. They concluded that metallicity could be a secondary effect. Gallagher et al. (2008) reported a correlation between age and optical luminosity and between HR and the metal abundance for early type galaxy hosts using diagnostic grids of spectral indices to determine the age and metallicity. Howell et al. (2009) were unable to reproduce the latter result using data from the Supernova Legacy Survey (SNLS). They used spectral energy distribution (SED) fitting to detrmine the galaxy masses and the Tremonti et al. (2004) relation to convert to metallicity. Howell et al. (2009) did find a correlation between the SN ^{56}Ni mass (determined from the peak bolometric luminosity of the SN) and the luminosity-weighted age of the host. For nearby SNe (Kelly et al. 2010) as well as more distant SNe with SNLS data (Sullivan et al. 2010) and SDSS-II data (Lampeitl et al. 2010), a relationship was found between the light curve shape-corrected SN luminosity and the mass of the host galaxy (estimated from SED fitting). D'Andrea et al. (2011) found significant differences when correlating HR with the gas phase metallicity or the specific star formation rate. The underlying source of the correlations is unclear, as the host galaxy mass, metallicity, and star formation are all connected together. Hayden et al. (2013) compare the residual scatter after correcting for mass alone and after correcting using the fundamental metallicity relation (which incorporates mass and star formation). They find the fundamental metallicity relation provides a significantly better correction and conclude that metallicity is the primary cause of the SN variations. Childress et al. (2013) find HR differences at low and high host mass with a sharp break in between. They argue that dust and progenitor age could also explain the differences.

Despite the larger expected differences in the UV, tests at those wavelengths have lagged behind due to the relative paucity of UV SN data compared to that available in the optical. Rest-frame near-UV (NUV) spectra of local SNe were compared to more distant samples by Riess et al. (2007), using rest-frame NUV spectra of $z \sim 1.1$ SNe observed with *Hubble Space Telescope* (*HST*). Ellis et al. (2008), using $z \sim 0.5$ SNe from SNLS, Foley et al. (2008) using $z \sim 0.5$ SNe from ESSENCE, and Foley et al. (2012a), using $z \sim 0.2$ SNe from SDSSII. In constructing a mean spectrum, all noted an increase in the average flux level in the UV and an increase in the dispersion at shorter wavelengths. Ellis et al. (2008) found the variations to be larger than that expected from metallicity differences as modeled by Lentz et al. (2000). Foley et al. (2008) noted that the blueshifted Si II 6355 Å would indicate higher metallicity (Lentz et al. 2000), the weaker Fe III 5129 Å line could indicate lower metallicity (Höflich et al. 1998; Sauer et al. 2008), and the higher UV flux level could indicate higher

(Höflich et al. 1998) or lower metallicity (Lentz et al. 2000; Sauer et al. 2008). UV photometric studies showed a modest increase in scatter at NUV wavelengths (Brown et al. 2010; Wang et al. 2012; Milne et al. 2013) and a large dispersion in the mid-UV (MUV) (Brown et al. 2010). Recently, Foley & Kirshner (2013) presented a relative metallicity determination between two SNe Ia based on UV spectra from *HST* which was further discussed in Graham et al. (2015).

In examining the possibility of evolution in SNe Ia, Howell et al. (2007) and Sullivan et al. (2009) find modest evolution in the optical properties which may be of concern when much higher accuracies are demanded to differentiate dark energy models. Sullivan et al. (2009) also find a UV flux difference between the low-z and intermediate-z SN samples, but the nearby sample only had 3 spectra within the SN stretch and epoch cuts. Cooke et al. (2011) and Maguire et al. (2012) used a much larger sample of NUV spectra from *HST*, confirming the earlier results. Additionally, Maguire et al. (2012) used the models from Walker et al. (2012) to conclude that the magnitude of both the dispersion and evolution were consistent with variation and evolution in the metallicity. Milne et al. (2015) categorize local and distant SNe Ia based on the NUV-blue/red dichotomy demonstrated in Milne et al. (2013). They find that the systematic differences in the UV flux of nearby and distant SNe Ia discussed above results not from a shift in the color distribution but a shift in the relative fractions of type Ia belonging to these two groups whose color distributions are similar across redshifts.

With high quality UV spectra from *HST* and a large photometric sample from *Swift*/ UVOT, it seems timely to assess some of the SN models and how they relate to now available observations. In Section 2 we will discuss the observational sample. The theoretical models to be utilized will be described in Section 3. In Section 4 we will compare the observations to the models using colors and color differences. Our conclusions are summarized and discussed in Section 5.

2. ULTRAVIOLET OBSERVATIONS

For our observational sample, we utilize observations of SNe Ia from the *Swift* Ultra-violet/Optical Telescope (Gehrels et al. 2004; Roming et al. 2005). We use SNe previously published (Brown et al. 2009, 2012a, 2012b; Milne et al. 2010, 2013), but updating the previously published photometry as necessary with the revised UV zeropoints and sensitivity degradation from Breeveld et al. (2011). This is done as part of the *Swift* Optical/Ultraviolet Supernova Archive (SOUSA; Brown et al. 2014a). The updated photometry is available from the *Swift* SN website.[6] We limit the sample to normal SNe (i.e., no SN 1991 T-like, 1991bg-like, or 2002cx-like SNe) with $1.0 < \Delta m_{15}(B) < 1.4$ observed with *Swift* at the time of the *B* band maximum light. This cut is done for two reasons. First, the models under consideration were based on normal SNe and thus are not as applicable for the other subtypes. We do not want color differences that might correlate with $\Delta m_{15}(B)$ to be confused with the color differences from metallicity. Second, our metallicity concerns focus on normal SNe that are useful for cosmology. We do not correct for extinction, but will use color–color plots and reddening vectors to show the effect it will have.

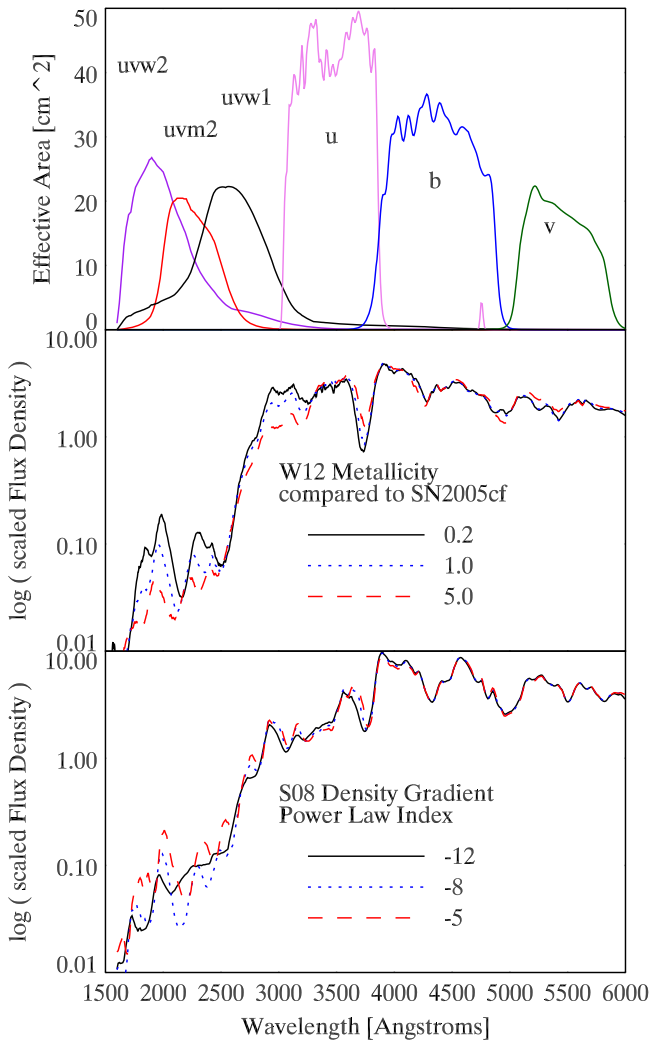6 http://swift.gsfc.nasa.gov/docs/swift/sne/swift_sn.html

Figure 1. Top panel: *Swift* UVOT filter curves. Middle panel: theoretical spectra from Walker et al. (2012) for which the metal content has been scaled (as indicated) relative to the best-fit model for SN 2005cf. Bottom panel: theoretical spectra from Sauer et al. (2008) for which the outer density gradient has been parameterized by a power-law with the indicated index.

We also use NUV spectra obtained with the *HST* Space Telescope Imaging Spectrograph (STIS) of SNe 2011by and 2011fe (GO-12298; PI: R. Ellis; Mazzali et al. 2014) as used by (Foley & Kirshner 2013) and (Graham et al. 2015).

For comparison with the observations, spectrophotometry on the *HST* spectra and model spectra in the UVOT photometry system use the revised effective area curves and zeropoints of Breeveld et al. (2011). The wavelength range of the filters is shown in the top panel of Figure 1. The spectrophotometry naturally includes the red tails of the *uvw*2 and *uvw*1 filters which transmit a significant amount of optical light when observing very red sources. In Brown et al. (2010) an approximate correction (equivalent to an s-correction to an idealized filter with the tails truncated) was utilized to study the dispersion of absolute magnitudes in the UV as might be observed at higher redshift with an optical filter with a sharper transmission cutoff. Such corrections can be highly uncertain because they require a spectrum to be assumed or modeled in order to determine the relative fraction coming from the UV and optical portions of the spectrum. In comparing with model spectra, such corrections are unnecessary as spectrophotometry
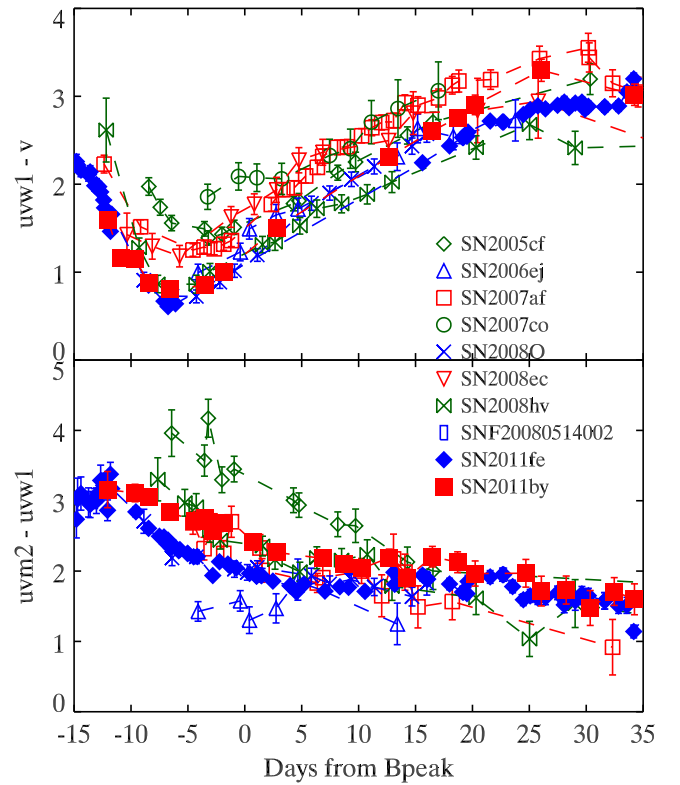

Figure 2. Color curves of SNe 2011by and 2011fe along with other young, normal SNe Ia (Brown et al. 2014b). The *uvw*1 − *v* colors of SNe 2011by and 2011fe are very similar. The *uvm*2 − *uvw*1 colors of SNe 2011by and 2011fe are distinct (but small) at all times, but the difference becomes smaller with time.

will include the effects of the optical tails. Differences that exist solely in the UV may be diluted by the optical flux, but we show below that the *uvw*2 and *uvw*1 still provide unique information. In the following we will refer to wavelengths between 2500–4000 Å (including the UVOT *u* and *uvw*1 filters) as the NUV and 1600–2600 Å (including the *uvw*2 and *uvm*2 filters) as the MUV. UVOT's optical filters are *b* and *v* (4000–6000 Å). For our broad color comparisons we will use *uvm*2 to represent the MUV (because it has very low sensitivity to optical photons), *uvw*1 to represent the NUV (due to several bright SNe Ia being at or above the saturation limit in *Swift's u* band), and *v* band to represent the optical (for the broadest wavelength coverage). Other filter choices would give the same general conclusions, and the wavelengths of certain features would make certain filter combinations particularly advantageous.

In Figure 2 we show the *Swift*/ UVOT colors of a representative sample of SNe. To facilitate comparisons with Foley & Kirshner (2013), we highlight the colors of SNe 2011by and 2011fe, which show the same characteristics reported from the spectra: the optical and NUV light curves and colors are very similar, differing only in the epochs more than five days before the *B* band peak. In the MUV, SN2011fe is consistently bluer. This difference is qualitatively similar to the colors and absolute magnitudes studied by Milne et al. (2010) and Brown et al. (2010), namely, a low dispersion in the optical and NUV, and an increased dispersion in MUV *uvm*2 and *uvw*2. The growing *Swift* SN sample shows there could also be a significant variation or bimodal distribution in the NUV-optical colors (Thomas et al. 2011; Milne et al. 2013). In this
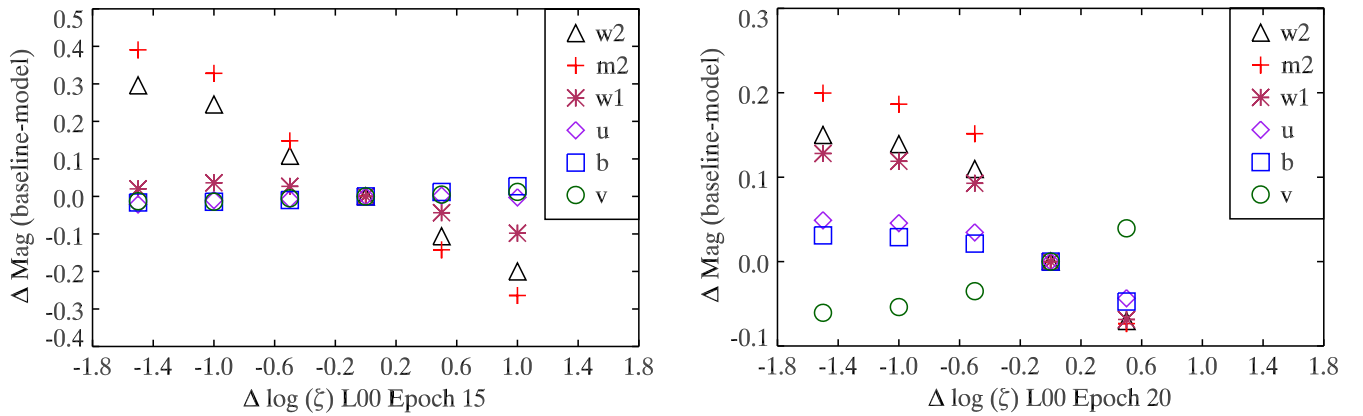
Figure 3. Left: magnitude differences in the UVOT filters for the Lentz et al. (2000) models at 15 days after explosion. These are spectrophotometric magnitudes computed from the model spectra subtracted from the baseline measurements to highlight the differences. Positive values indicate an increase in flux in that filter relative to the baseline model. Right: magnitude differences in the UVOT filters for the Lentz models at 20 days after explosion. While the largest differences are still in the MUV filters, there is also significant change in the other filters.

paradigm, SNe 2011by and 2011fe are both classified as NUV-blue SNe (Milne et al. 2013). Compared to the larger sample of SNe, SNe 2011by and 2011fe are quite similar in the MUV as well, as the MUV differences between SNe 2011by and 2011fe are small compared to the large scatter seen between other objects. It is the cause of these similarities and differences which we wish to explore with various theoretical models.

3. THEORETICAL MODELS

As described in Section 1, many different groups have examined the differences which metallicity and other parameters have on SN observables. Here we describe in more detail five sets of models for which we have spectra for our comparisons: Lentz et al. (2000), Sauer et al. (2008), Walker et al. (2012), Blondin et al. (2013), and Kromer & Sim (2009). We will refer to these hereafter as L00, S08, W12, B13, and K09, respectively.

The L00 models begin with a W7 deflagration model (Nomoto et al. 1984; Thielemann et al. 1986). The radiative transfer calculations were performed with the PHOENIX code (Hauschildt et al. 1996; Hauschildt & Baron 1999). The models are given at epochs 7, 10, 15, 20, and 35 days after explosion, with luminosity parameters modified to fit optical (not UV) spectra of SN 1994D at -12, -9, -4, 0, and 15 days after B band maximum light. The metallicity is changed by scaling the number abundance of elements heavier than oxygen in the outer, unburned C+O layer (velocities 14,800–30,000 km s^{-1}) by a factor ζ between 1/30 and 10. They then renormalize the mass fractions in each layer. To simulate the nucleosynthetic effect of metallicity changes, they also scale the amount of ^{54}Fe in the incomplete burning zone (8800–14,800 km s^{-1}) in the same way. Considering the effects separately, the element abundances in the unburned layer have a much stronger effect on the observed spectra. Here we use the model spectra where both of these effects are combined, parameterized by the scaling factor ζ.

Figure 3 shows the spectrophotometry of models corresponding to 15 and 20 days after explosion. These and the other model plots show the model photometry subtracted from the baseline model photometry to quantify the differences. In the day 15 models the MUV brightness increases as ζ decreases (corresponding to a lower heavy element abundance in the outer layer). The changes to the optical and NUV are

negligible, consistent with the flux ratios shown by Foley & Kirshner (2013). In the right panel, the day 20 models (corresponding to the maximum light epoch of SN 1994D) the changes are more modest and affect all of the filters but with the effect strongest at shorter wavelengths.

S08 used the density structure W7 deflagration model (Nomoto et al. 1984; Thielemann et al. 1986) and the Monte-Carlo radiative transfer code of Mazzali & Lucy (1993). This includes the line-branching formalism and reverse flourescence from Lucy (1999) and Mazzali (2000). The composition and luminosity were tuned so that the emergent spectra matched the UV/optical spectra of SNe 2001eh and 2001ep at 9 days after B-peak (the epoch of the *HST* UV spectra). Here we use the models of the moderately declining ($\Delta m_{15}(B) = 1.41$) SN 2001ep. The effect of metallicity is probed by changing the abundance of certain elements in the outermost zone with velocities above 14,500 km s^{-1} (extending to 70,000 km s^{-1}) at the expense of oxygen. They modify the stable Fe, ^{56}Ni, and Ti and Cr together. Of these, ^{56}Ni has the strongest effect in the MUV, though each has a unique signature in the spectral differences which also shows up in the broadband photometry. Figure 4 shows the relative spectrophotometry for the Fe and ^{56}Ni models. In the left panel, decreasing the amount of Fe has little effect at any wavelength, but the u and $uvm2$ bands are brighter (and the b band fainter) for larger amounts of Fe. This increase in UV flux is attributed to a larger number of saturated Fe lines encouraging reverse fluorescence. In the right panel, the MUV filters are brighter for lower amounts of Ni. As the amount of Ni is increased, the u band is brighter while the MUV and b bands are fainter. The fact that filters with significant overlap can move in different directions shows that some of the effects are restricted to narrow bands in wavelength.

S08 also compute spectra for different density structures resulting from different explosion models (W7, WDD2, and DD4) and with the density of the outer layers modeled as a power-law with a varying index. WDD2 (Iwamoto et al. 1999) and DD4 (Woosley & Weaver 1994) are delayed detonation models. The relative spectrophotometry is shown in Figure 5. The NUV flux is significantly weaker for the DD4 and WDD2 models compared to W7. For varying density profiles, the NUV flux is strongly enhanced for shallower profiles but also enhanced for steeper profiles. Clearly the density profile has a
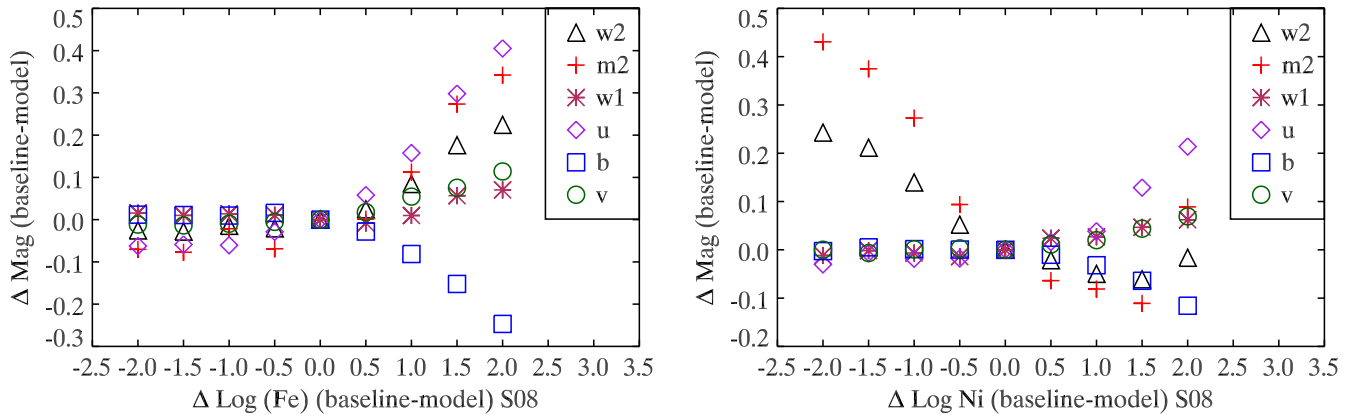
Figure 4. Magnitude differences for different forms of metallicity variations (S08). These are spectrophotometric magnitudes computed from the model spectra subtracted from the baseline measurements to highlight the differences. The left panel shows the differences varying the amount of Fe. The right panel shows the differences from varying ^{56}Ni abundances. In both cases the UV is much more strongly affected than the optical, but the filters are affected by different amounts for the different variations.
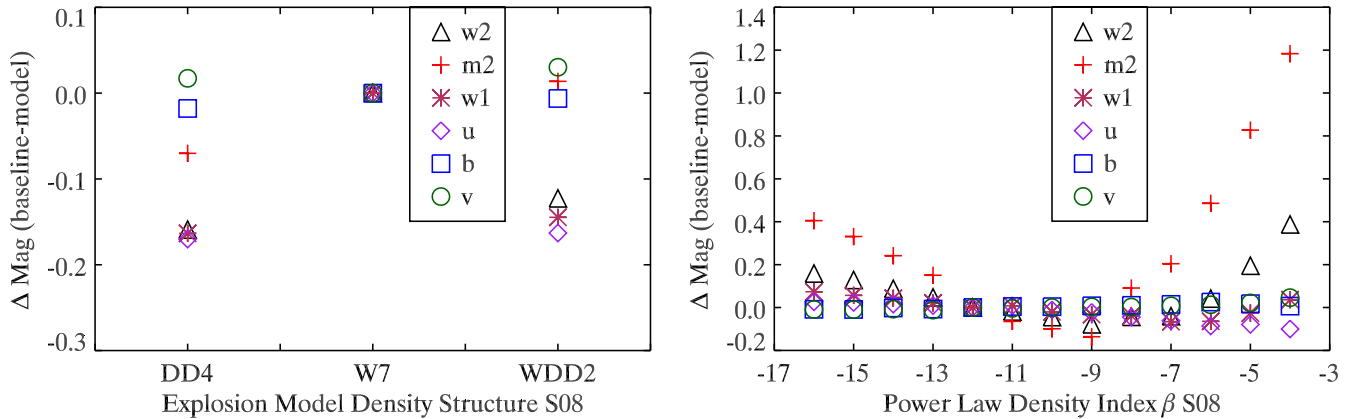

Figure 5. Left: magnitude differences in the UVOT filters for the S08 models using the density structure from different explosion models. These are spectrophotometric magnitudes computed from the model spectra subtracted from the baseline measurements to highlight the differences. Right: magnitude differences in the UVOT filters for the S08 models with the density structure of the outer layers parameterized by a power-law with a variable index. To isolate the effect of changing the slope of the outer density structure, the $\beta = -12$ model is used as the baseline for this comparison. Only the mid-UV (*uvw*2 and *uvm*2) filters are affected.

strong but nonlinear effect on the MUV luminosity. The wavelength where the differences show up—the explosion models affecting the NUV and the varying power law in the outer density affecting the MUV—might prove an important diagnostic in constraining the true density structure. Mazzali et al. (2014) had to modify the standard explosion model density structure to fit the UV spectra of SN 2011fe.

The W12 models use the density profile of the W7 deflagration model and delayed detonation models WDD1 and WDD3 (Iwamoto et al. 1999) depending on the luminosity/Ni mass produced. The radiative transfer is done with a Monte-Carlo code (Mazzali & Lucy 1993). Using an abundance tomography approach (Stehle et al. 2005) to model the UV/optical observations of SN 2005cf, many premaximum epochs are utilized to constrain abundances in the outer layers to create the near-maximum model matched to the observations 0.9 days before *B*-band maximum. The metallicity is changed by scaling the abundances of all elements with atomic number above calcium by a factor η ranging between 0.05 and 5. The mass fractions are similarly scaled at the expense of unburnt C/O. This is done in the outer three layers of the model, corresponding to velocities greater than 13,100 km s^{-1} for the luminosity $\log(L_{\rm bol}/L_\odot) = 9.6$ model. Plots showing the effect

from changing single elements are also given in Walker et al. (2012). They also create models with varying luminosity corresponding to different energies and ^{56}Ni production.

The left panel of Figure 6 shows the effect of changing the metal abundance in the outer layers. For lower metal abundance the MUV filters and the NUV *uvw*1 filter are brighter, while increasing the metal abundance lowers the flux in those filters. The right panel shows the different luminosity models. This is clearly reflected in the magnitude differences of about 1.6 mag for most filters. The lowest luminosity model also shows a significant chromatic difference with the *uvw*1 relatively fainter and the *uvm*2 relatively brighter. Note how the effects cancel each other out leaving the *uvw*2 magnitude unchanged.

B13 uses a forward modeling approach with a grid of one-dimensional Chandrasekhar-mass delayed detonation models as in Khokhlov (1991). The density at which the transition from deflagration to detonation is varied, resulting in differing amounts of ^{56}Ni. The radiative transfer was done using the CMFGEN code (Hillier & Miller 1998; Hillier & Dessart 2012). From a larger grid, eight models were published in B13 which matched observed spectra. Figure 7 shows the model magnitude differences with respect to the DDC10 model
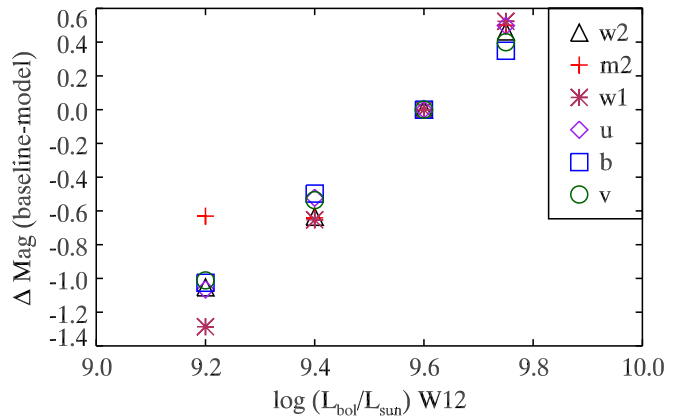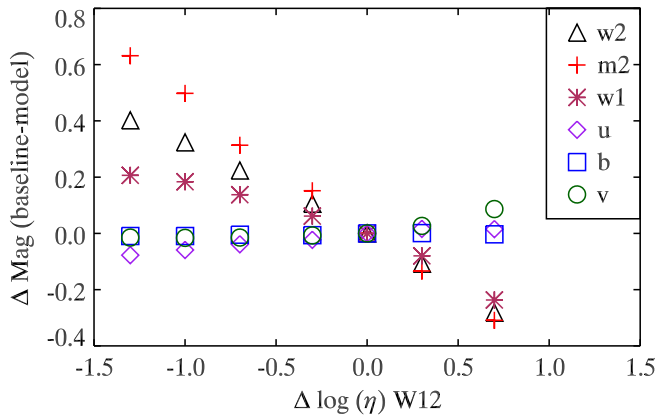
Figure 6. Left: magnitude differences in the UVOT filters for the Walker models (with fixed $\log(L) = 9.6$) with varying metallicity. These are spectrophotometric magnitudes computed from the model spectra subtracted from the baseline measurements to highlight the differences. Right: magnitude differences in the UVOT filters for the Walker models with varying luminosity and a fixed metallicity.
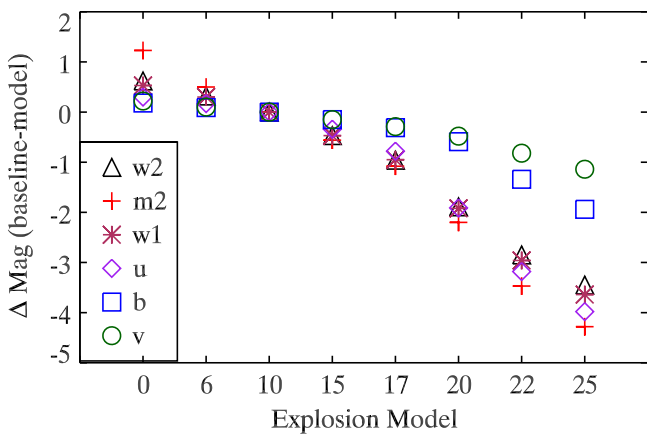

Figure 7. Magnitude differences (compared to the DDC10 model) for different 1D delayed-detonation models (Blondin et al. 2013). See Blondin et al. (2013) for details about the numbered models. Changing ^{56}Ni has a modest effect on the optical colors compared to the larger effect on the near-UV and mid-UV filters.

Figure 8. Magnitude differences for different viewing angles for an ellipsoidal toy model (Kromer & Sim 2009).

which was found to be a good match to SN 2005cf (the same SN on which the W12 baseline model was based). Compositions are not varied, but one can see how the different wavelength regions are effected by the change in ^{56}Ni. The UV is much more sensitive than the optical to differences in ^{56}Ni. Though beyond the scope of this paper, this shows how UV photometry of SNe spanning a range ^{56}Ni can either guide the creation of models or be used with accurate models to independently determine ^{56}Ni from UV-optical colors. Foley et al. (2012b) found strong differences in the UV spectra of a few type Ia SNe with differing $\Delta m_{15}(B)$ (as a proxy for ^{56}Ni).

K09 use an ellipsoidal toy model to explore how the viewing angle of an asymmetric explosion will change the observed properties. K09 stresses the simplicity and extreme asphericity of the model. As in K09, we are also less interested in the magnitude of the effect but the relative strength it has on the different filters. We use the spectral output at maximum light. Figure 8 shows the differences in magnitude as a function of viewing angle, such that $0°$ corresponds to viewing down the semimajor axis and $90°$ views down on the equator. The effect on the magnitudes is less chromatic than for the other models considered. There is an overall luminosity variation, related to the observed cross section (K09). The spectrum blueward of 4000 Å is more strongly affected, so
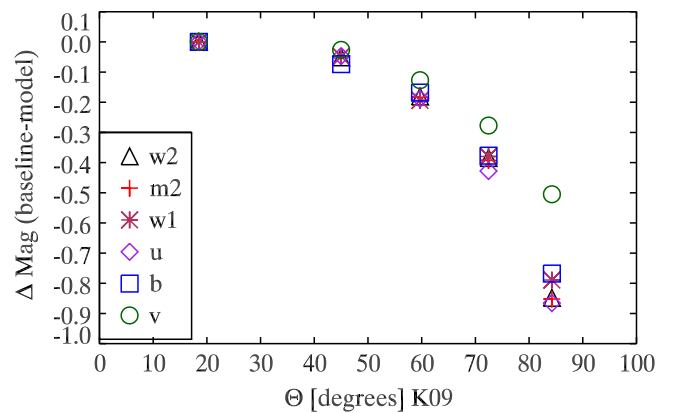
the v band is affected less than the others. Thus $B − V$ or NUV$−V$ colors are affected, but MUV–NUV much less so.

Before comparing to observations we emphasize that L00 and B13 took a forward modeling approach while the S08 and W12 models were modified to individual SNe with UV observations. They do not represent all SNe Ia, but we test how well changing the models relative to them reproduces the variation observed in SNe. We also note that the models considered in this paper do not represent a full sample of the models considered in the literature. They are not even a full sample of the models considered in the above five studies. The models used represent the most applicable models available to us. To allow for comparison, it might be profitable to establish an online database of models comparable to the observational databases currently available via SUSPECT[7], WISERE-P[8](Yaron & Gal-Yam 2012), and the CfA[9] and Berkeley/Filippenko Group SN archives[10] (Silverman et al. 2012). The useful outputs to share might range from the density structures used as input to the output spectra and light curves. To allow theoretical models to be compared with our data, we make our

---

[7] http://bruford.nhn.ou.edu/~suspect/index1.html
[8] http://www.weizmann.ac.il/astrophysics/wiserep/
[9] http://www.cfa.harvard.edu/supernova/SNarchive.html
[10] http://hercules.berkeley.edu/database/index_public.html
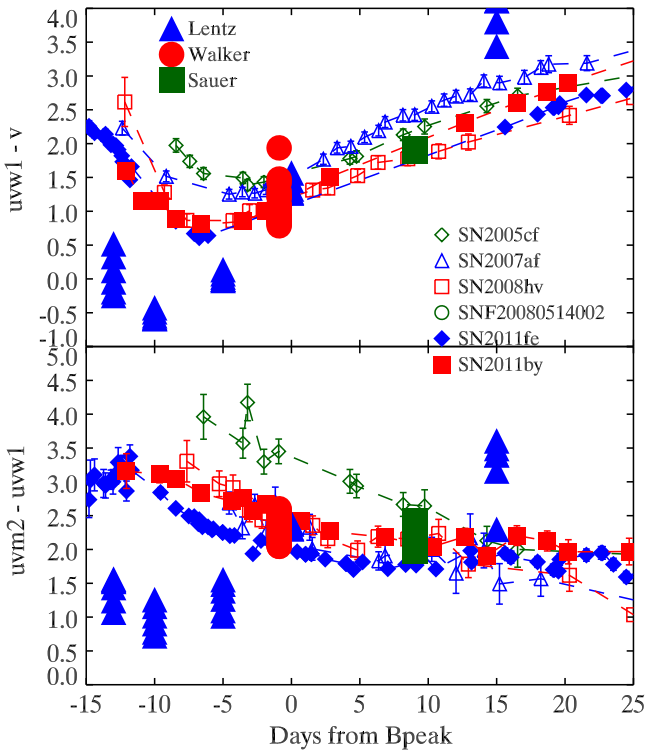
Figure 9. Color evolution as observed for *Swift*/ UVOT SNe and as predicted by various models. The color evolution of the Lentz models is faster, stronger and offset from that observed. The colors of the Walker and Sauer models match most of the SNe (having been tuned to actual observations) but with a scatter inconsistent with the observations. The dispersion in colors and different epochs should constrain the variation of different model parameters.

SOUSA photometry available on the *Swift* SN home page[11] (Brown et al. 2014a).

4. RESULTS

4.1. Colors

The models of Lentz et al. (2000) are at epochs of 7, 10, 15, 20 and 35 days after explosion. The model spectrum at 20 days was matched to a maximum light spectrum of SN 1994D, so we use that to shift the epochs from days after explosion to days from maximum light. The Walker et al. (2012) and Sauer et al. (2008) models were run for epochs of -1 and 9 days after B maximum, respectively, based on the epochs of the spectra available to them. We compare the models to the *Swift*/ UVOT observations described above in $uvm2 - uvw1$ and $uvw1 - v$. Figure 9 plots the color evolution of the *Swift* SNe Ia to the varying-metallicity models L00, S08, and W12. The scatter in the models is created by the variations in metallicity—only single SNe were modeled in each case.

The early epoch models of Lentz et al. (2000) are about one magnitude too blue in both colors and evolve much faster, but the shape of the $uvw1 - v$ color evolution is qualitatively similar to the observations. We emphasize that these models were matched to optical spectra and then modified to explore the differences in metallicity. The Lentz et al. (2000) W7 models were not based on UV spectra and are much bluer than observations (e.g., SN 1992A; Kirshner et al. 1993) or more recent models (compare Figures 1–3 in Baron et al. 2006).
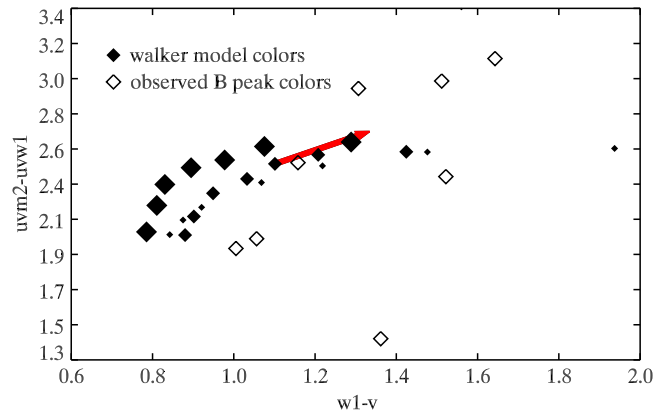
Figure 10. Color–color plot of the models and observations. The predicted colors of the Walker et al. (2012) models are shown with large, medium and small solid symbols, covering a the range of metallicity discussed above for three different luminosities corresponding to $\log(L_{bol}/L_\odot) = 9.75$, 9.6, and 9.4, respectively. Metallicity increases to the right, though the individual values matter less than the relative location of the models and observations. The *Swift*/ UVOT observed colors at peak are plotted as open symbols. An arrow shows the reddening vector for the Milky Way (Cardelli et al. 1989) extinction law with $E(B - V) = 0.1$. The observed colors show a larger scatter than the models but not in a manner consistent with reddening.

Metallicity variations in W7 have been more thoroughly studied and compared to the UV-IR spectra of SN 2011fe (M. Jenks et al. 2015, in preparation). The Walker et al. (2012) and Sauer et al. (2008) models were based on observed UV spectra and better match the observed colors. For this study we are less interested in the actual colors but rather the scatter in the observed colors and whether it could be accounted for by the variation in model colors. The spread of the L00 and W12 models are similar to the spread of the observed $uvw1 - v$ colors. This is consistent with the finding of Maguire et al. (2012) that the scatter in their NUV spectra was consistent with metallicity variations from W12. The W12 models do not cover the spread in the $uvm2 - uvw1$ colors. The L00 and W12 models also underpredict the scatter in the $uvm2 - uvw1$ colors at maximum light. The $uvm2 - uvw1$ colors of the observations and S08 models are quite comparable at 9 days after max where the observed $uvm2 - uvw1$ colors are more uniform, but the S08 models underestimate the $uvw1 - v$ scatter. Multi-wavelength observations constrain how much scatter in one color can be reproduced by one parameter variation without creating too much scatter in another color. Some additional scatter could be the result of extinction, though we see SNe which are bluer than most of the models. Color–color vectors could differentiate the effects. As shown in Figure 10, the metallicity differences redden the colors in a manner generally similar to dust reddening, but bluer observed colors suggest intrinsic differences beyond that explored by the models.

4.2. Flux Ratios

To see the difference between two SNe or among a group of SNe, one can divide the flux of one by the flux of the other. This can be done with models as well. We are then concerned not with the absolute colors and metallicities, but the color differences and relative metallicity ratios between models or objects. For the Lentz et al. (2000) models, the composition of the W7 model is changed by scaling the number abundances of elements heavier than oxygen. The composition is scaled by factors ranging from 10 to 1/30, yielding a total range of 300
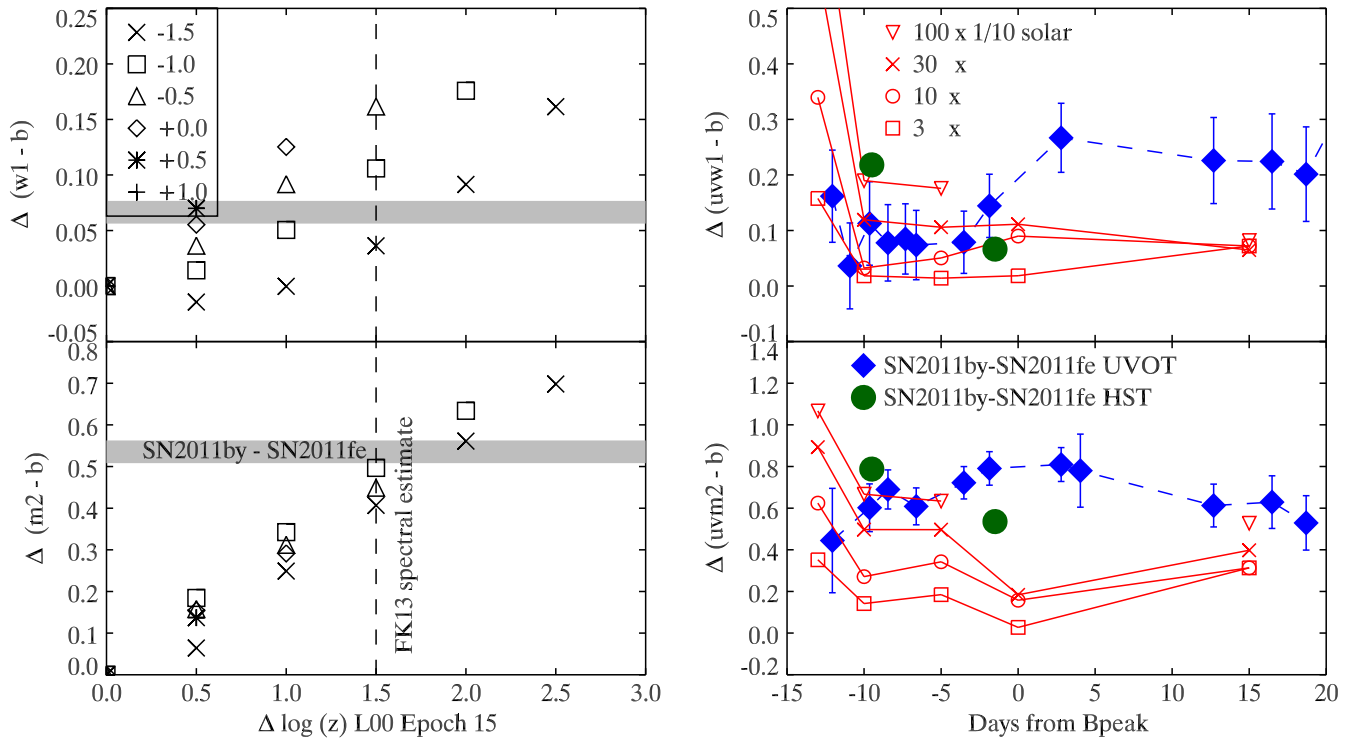
Figure 11. Left panel: color differences between the L00 day 15 models vs. the metallicity difference between the models. Each of the models is compared to those of higher (as well as itself, resulting in the points at 0,0). The baseline (lower metallicity) models used in the comparisons are differentiated by symbols, though the individual points are not important. What is of interest is the effect on the relative colors resulting from a difference in the metallicity. The vertical dashed line represents the metallicity difference between SNe 2011by and 2011fe of ∼30 inferred by Foley & Kirshner (2013) from *HST* UV spectra. The horizontal line represents the color difference of the SNe at peak based on spectrophotometry. The intersection of the models and $uvm2 - uvw1$ colors show that a comparable metallicity differential could be obtained from $uvm2 - b$ photometry alone. For extreme metallicity differences, the absolute metallicity could also be determined with $uvw1 - b$ color errors smaller than 0.05 mag. Right panel: the temporal evolution of the color differences are compared to the UVOT and *HST* spectrophotometric color differences between SNe 2011by and 2011fe. The relative differences of the models are consistent before maximum light. At and after maximum light, however, the observed color differences are not consistent with the Lentz et al. (2000) models.

(∼2.5 dex) in the ratios of the highest metallicity model to the lowest (or 1/300 if reversed). Foley & Kirshner (2013) and Graham et al. (2015) used this flux ratio method to attribute the difference between SNe 2011by and 2011fe to a metallicity ratio of 1/30 based on the models of Lentz et al. (2000). Pan et al. (2015) performed similar comparisons for SN 2013dy though they also found spectroscopic differences not consistent with the metallicity models. While some groups have examined the effects on individual line strengths and locations (Walker et al. 2012), most of the comparisons with observations have relied on broader spectral shapes (Maguire et al. 2012; Foley & Kirshner 2013). Such broad spectral shapes can also be measured using photometry. For one such implementation, we use similar colors as above comparing the MUV to NUV and NUV to optical: $uvm2 - uvw1$ and $uvw1 - b$. The b band is used here because the *HST* spectra of SN 2011by do not fully cover the v band. The color difference between any two models separates out the color effects as a function of the model parameter changed. The left panel Figure 11 shows the color differences for the day 15 L00 models (each subtracted from lower metallicity) as a function of the metallicity ratio between the two. As reported by Foley & Kirshner (2013), the flux ratios in the MUV are similar between models with the same metallicity ratios regardless of the absolute metallicity. The dotted vertical line shows the metallicity ratio inferred by Foley & Kirshner (2013) from dividing the SN 2011fe spectrum by the SN 2011by spectrum and comparing with the spectral flux ratios of the Lentz models.

The horizontal line shows the color difference of SNe 2011fe and 2011by from *HST* just before maximum light (the same spectra used by Foley & Kirshner 2013). The $uvw1 - b$ colors of the models contain too much scatter without knowing the absolute metallicity of one of the objects and are consistent with a large spread in metallicity difference with relative metallicity ratios ranging from 3 to 50. The metallicity difference inferred from the photometry would be a factor of 100, and uncertainties of a few percent in the colors would also allow the FK13 estimate of 30.

The fact that the two lines and the model photometry differences intersect at the same place suggests that UV photometry could put the same constraints on the metallicity differences between SNe as the rarer and harder to obtain UV spectra. This result assumes that the model differences are the same as those in the SNe. Such a comparison might also require further optical photometry and spectra to identify SN pairs which are otherwise similar. The photometric comparison does miss out on small scale differences due to varying line or continuum flux, but so did the spectral comparison of Foley & Kirshner (2013). Studying small scale differences in UV spectra might better reveal the origin of the differences. The UV photometric differences could then constrain the magnitude of the differences.

Graham et al. (2015) found that a comparison of the premaximum spectra of SNe 2011by and 2011fe were also consistent with a 1/30 ratio of metallicities. With the larger temporal coverage of the UVOT photometry of SNe 2011by

and 2011fe we can compare the post-maximum behavior. Similar to the left panel, the right panel of Figure 11 shows relative color differences between the models and the observations. The day 20 spectral models of Lentz et al. (2000) which were modeled to a maximum light spectrum of SN 1994D show a much depressed variation in the MUV. The post-maximum behavior is also very different than observed. While this photometric method appears promising, the Lentz et al. (2000) models do not accurately reflect the colors in an absolute or relative sense.

5. SUMMARY

In this paper we have shown the photometric effect of changing the metallicity (Lentz et al. 2000; Sauer et al. 2008; Walker et al. 2012), density structure (Sauer et al. 2008), explosion model (Blondin et al. 2013), and asymmetry (Kromer & Sim 2009) of SN Ia models. Metallicity and density structure changes cause photometric differences which generally increase at shorter wavelengths, while asymmetry changes affect the $B - V$ color and are flat blueward of B. Compared to *Swift* SNe, the predicted scatter from metallicity variations is smaller than what is observed, particularly in the MUV. The older Lentz et al. (2000) models do not predict the color evolution very well, but the temporal differences in the colors and color dispersion suggest multi-epoch modeling and predictions to be an attractive way to resolve degeneracies in the many parameters which effect the UV flux.

Ignoring the absolute color differences in the Lentz et al. (2000) models, we explore how color differences between SNe could be used to measure metallicity differences as has been claimed for UV spectra (Foley & Kirshner 2013). We find the photometric differences between SNe 2011by and 2011fe give the same metallicity differences as the spectra when using the same pre-maximum light models. The near-peak models form Lentz et al. (2000), however, underpredict the MUV differences. The Lentz et al. (2000) models do not reproduce the color differences from multi-epoch photometric comparisons. While metallicity may indeed be the difference between these similar SNe, the difference found by Foley & Kirshner (2013) and Graham et al. (2015) is not supported by our observations. Here we have followed Foley & Kirshner (2013) in assuming that the color differences between SNe 2011by and 2011fe are solely caused by a single parameter under investigation. The photometric tests show that a number of different parameters strongly affect the UV light. The large UV dispersion seen in SN observations is likely the product of multiple effects. With improved models, however, time-series comparisons (with photometry or spectroscopy) might prove very effective in quantifying physical differences between SNe or their progenitors and showing which differences are observationally degenerate.

There is a modest observed difference in the NUV-optical colors which persists past maximum light (Milne et al. 2013). There is a large observed dispersion in the MUV–NUV colors which is strongest at early times (Brown et al. 2014b). As we have shown here, theory also predicts many intrinsic differences in SNe Ia result in strong signatures in the UV with different wavelength ranges and time scales (see also Höflich et al. 2013 and Sadler et al. 2013). Understanding the temporal changes is an important step in understanding the differences among SNe Ia to conclusively link observed behavior with specific physical differences. Historically,

detailed modeling of SNe relied on high-quality, single epoch UV spectra. The superbly sampled UV observations of SN 2011fe (Mazzali et al. 2014) allowed the energetics, density structure, and metallicity to be very well constrained. Mazzali et al. (2014) also found the sub-solar metallicity to be consistent with that of the host galaxy (Stoll et al. 2011), making it a rough zeropoint in translating UV colors to absolute metallicities. Modifying those parameters (similar to Lentz et al. 2000; Sauer et al. 2008 and Walker et al. 2012) and following the resultant differences in the UV colors would clarify what could make SN 2011by appear so similar in the optical and yet different in the UV (Foley & Kirshner 2013). It would also help us better understand the UV differences for the larger sample of SNe observed photometrically in the UV. Despite the larger photometric sample, additional UV spectral series are needed in order to map out the variations in observed properties.

Understanding the UV light of SNe Ia has important implications for their use as cosmological tools. Since the UV is sensitive to many effects, it can be used to probe changes with redshift in metallicity or dust properties. The higher leverage in the UV can test for differences which would effect at a smaller level the rest-frame optical/NIR (which are used for the cosmological measurements). Strong apparent differences in the rest-frame NUV-optical colors have been found by Milne et al. (2015) increasing with redshift. A better physical understanding of the UV differences is needed to understand how much the optical is affected and, if it is, how to correct it to improve the precision of cosmological measurements.

REFERENCES

Baron, E., Bongard, S., Branch, D., & Hauschildt, P. H. 2006, ApJ, 645, 480
Blondin, S., Dessart, L., Hillier, D. J., & Khokhlov, A. M. 2013, MNRAS, 429, 2127
Branch, D. 1998, ARA&A, 36, 17
Bravo, E., Domínguez, I., Badenes, C., Piersanti, L., & Straniero, O. 2010, ApJL, 711, L66
Breeveld, A. A., Landsman, W., Holland, S. T., et al. 2011, in AIP Conf. Ser. 1358, Gamma Ray Bursts 2010, ed. J. E. McEnery, J. L. Racusin & N. Gehrels (Melville, NY: AIP), 373
Brown, P. J., Breeveld, A. A., Holland, S., Kuin, P., & Pritchard, T. 2014a, A&SS, 354, 89
Brown, P. J., Dawson, K. S., de Pasquale, M., et al. 2012a, ApJ, 753, 22
Brown, P. J., Dawson, K. S., Harris, D. W., et al. 2012b, ApJ, 749, 18
Brown, P. J., Holland, S. T., Immler, S., et al. 2009, AJ, 137, 4517
Brown, P. J., Kuin, P., Scalzo, R., et al. 2014b, ApJ, 787, 29
Brown, P. J., Roming, P. W. A., Milne, P., et al. 2010, ApJ, 721, 1608
Cardelli, J. A., Clayton, G. C., & Mathis, J. S. 1989, ApJ, 345, 245
Childress, M., Aldering, G., Antilogus, P., et al. 2013, ApJ, 770, 108
Cooke, J., Ellis, R. S., Sullivan, M., et al. 2011, ApJL, 727, L35
D'Andrea, C. B., Gupta, R. R., Sako, M., et al. 2011, ApJ, 743, 172

Ellis, R. S., Sullivan, M., Nugent, P. E., et al. 2008, ApJ, 674, 51
Foley, R. J., Filippenko, A. V., Aguilera, C., et al. 2008, ApJ, 684, 68
Foley, R. J., Filippenko, A. V., Kessler, R., et al. 2012a, AJ, 143, 113
Foley, R. J., & Kirshner, R. P. 2013, ApJL, 769, L1
Foley, R. J., Kromer, M., Howie Marion, G., et al. 2012b, ApJL, 753, L5
Gallagher, J. S., Garnavich, P. M., Berlind, P., et al. 2005, ApJ, 634, 210
Gallagher, J. S., Garnavich, P. M., Caldwell, N., et al. 2008, ApJ, 685, 752
Ganeshalingam, M., Li, W., & Filippenko, A. V. 2013, MNRAS, 433, 2240
Gehrels, N., Chincarini, G., Giommi, P., et al. 2004, ApJ, 611, 1005
Graham, M. L., Foley, R. J., Zheng, W., et al. 2015, MNRAS, 446, 2073
Hauschildt, P. H., & Baron, E. 1999, JCoAM, 109, 41
Hauschildt, P. H., Baron, E., Starrfield, S., & Allard, F. 1996, ApJ, 462, 386
Hayden, B. T., Gupta, R. R., Garnavich, P. M., et al. 2013, ApJ, 764, 191
Hillier, D. J., & Dessart, L. 2012, MNRAS, 424, 252
Hillier, D. J., & Miller, D. L. 1998, ApJ, 496, 407
Höflich, P., Dragulin, P., Mitchell, J., et al. 2013, FrPhy, 8, 144
Höflich, P., Wheeler, J. C., & Thielemann, F. K. 1998, ApJ, 495, 617
Howell, D. A., Sullivan, M., Brown, E. F., et al. 2009, ApJ, 691, 661
Howell, D. A., Sullivan, M., Conley, A., & Carlberg, R. 2007, ApJL, 667, L37
Iwamoto, K., Brachwitz, F., Nomoto, K., et al. 1999, ApJs, 125, 439
Kelly, P. L., Hicken, M., Burke, D. L., Mandel, K. S., & Kirshner, R. P. 2010, ApJ, 715, 743
Khokhlov, A. M. 1991, A&A, 245, 114
Kirshner, R. P., Jeffery, D. J., Leibundgut, B., et al. 1993, ApJ, 415, 589
Kobayashi, C., Tsujimoto, T., Nomoto, K., Hachisu, I., & Kato, M. 1998, ApJL, 503, L155
Kromer, M., & Sim, S. A. 2009, MNRAS, 398, 1809
Lampeitl, H., Smith, M., Nichol, R. C., et al. 2010, ApJ, 722, 566
Leibundgut, B. 2001, ARA&A, 39, 67
Lentz, E. J., Baron, E., Branch, D., Hauschildt, P. H., & Nugent, P. E. 2000, ApJ, 530, 966
Lucy, L. B. 1999, A&A, 345, 211
Maguire, K., Sullivan, M., Ellis, R. S., et al. 2012, MNRAS, 426, 2359
Mazzali, P. A. 2000, A&A, 363, 705
Mazzali, P. A., & Lucy, L. B. 1993, A&A, 279, 447

Mazzali, P. A., & Podsiadlowski, P. 2006, MNRAS, 369, L19
Mazzali, P. A., Sullivan, M., Hachinger, S., et al. 2014, MNRAS, 439, 1959
Milne, P. A., Brown, P. J., Roming, P. W. A., Bufano, F., & Gehrels, N. 2013, ApJ, 779, 23
Milne, P. A., Brown, P. J., Roming, P. W. A., et al. 2010, ApJ, 721, 1627
Milne, P. A., Foley, R. J., Brown, P. J., & Narayan, G. 2015, ApJ, 803, 20
Nomoto, K., Thielemann, F.-K., & Yokoi, K. 1984, ApJ, 286, 644
Pan, Y.-C., Foley, R. J., Challis, P., et al. 2015, arXiv:1504.02396
Perlmutter, S., Aldering, G., Goldhaber, G., et al. 1999, ApJ, 517, 565
Riess, A. G., Filippenko, A. V., Challis, P., et al. 1998, AJ, 116, 1009
Riess, A. G., Strolger, L.-G., Casertano, S., et al. 2007, ApJ, 659, 98
Roming, P. W. A., Kennedy, T. E., Mason, K. O., et al. 2005, SSRv, 120, 95
Sadler, B., Hoeflich, P., Baron, E., et al. 2013, in IAU Symp. 281, Binary Paths to Type Ia Supernovae Explosion ed. R. Di Stefano, M. Orio & M. Moe (Cambridge: Cambridge Univ. Press), 309
Sauer, D. N., Mazzali, P. A., Blondin, S., et al. 2008, MNRAS, 391, 1605
Schmidt, B. P., Suntzeff, N. B., Phillips, M. M., et al. 1998, ApJ, 507, 46
Silverman, J. M., Foley, R. J., Filippenko, A. V., et al. 2012, MNRAS, 425, 1789
Stehle, M., Mazzali, P. A., Benetti, S., & Hillebrandt, W. 2005, MNRAS, 360, 1231
Stoll, R., Shappee, B., & Stanek, K. Z. 2011, ATel, 3588, 1
Sullivan, M., Conley, A., Howell, D. A., et al. 2010, MNRAS, 406, 782
Sullivan, M., Ellis, R. S., Howell, D. A., et al. 2009, ApJL, 693, L76
Suzuki, N., Rubin, D., Lidman, C., et al. 2012, ApJ, 746, 85
Thielemann, F.-K., Nomoto, K., & Yokoi, K. 1986, A&A, 158, 17
Thomas, R. C., Aldering, G., Antilogus, P., et al. 2011, ApJ, 743, 27
Timmes, F. X., Brown, E. F., & Truran, J. W. 2003, ApJL, 590, L83
Tremonti, C. A., Heckman, T. M., Kauffmann, G., et al. 2004, ApJ, 613, 898
Umeda, H., Nomoto, K., Kobayashi, C., Hachisu, I., & Kato, M. 1999, ApJL, 522, L43
Walker, E. S., Hachinger, S., Mazzali, P. A., et al. 2012, MNRAS, 427, 103
Wang, X., Wang, L., Filippenko, A. V., et al. 2012, ApJ, 749, 126
Woosley, S. E., & Weaver, T. A. 1994, ApJ, 423, 371
Yaron, O., & Gal-Yam, A. 2012, PASP, 124, 668